SUPPLEMENTAL DATA

Phytophthora infestans RXLR effector PexRD2 interacts with host MAPKKKε to suppress plant immune signalling

Stuart RF King[1], Hazel McLellan[2], Petra C Boevink[3], Miles R Armstrong[2], Tatyana Bukharova[2], Octavina Sukarta[2], Joe Win[4], Sophien Kamoun[4], Paul RJ Birch[2,3] & Mark J Banfield[1]

[1]Dept. of Biological Chemistry, John Innes Centre, Norwich Research Park, Norwich, NR4 7UH, UK, [2]Division of Plant Sciences, University of Dundee (at JHI), and [3]Cell and Molecular Sciences, James Hutton Institute, Invergowrie, Dundee, DD2 5DA, UK, [4]The Sainsbury Laboratory, Norwich Research Park, Norwich, NR4 7UH, UK

Correspondence to MJB: mark.banfield@jic.ac.uk

Running Title: PexRD2 interferes with MAPKKKε signalling

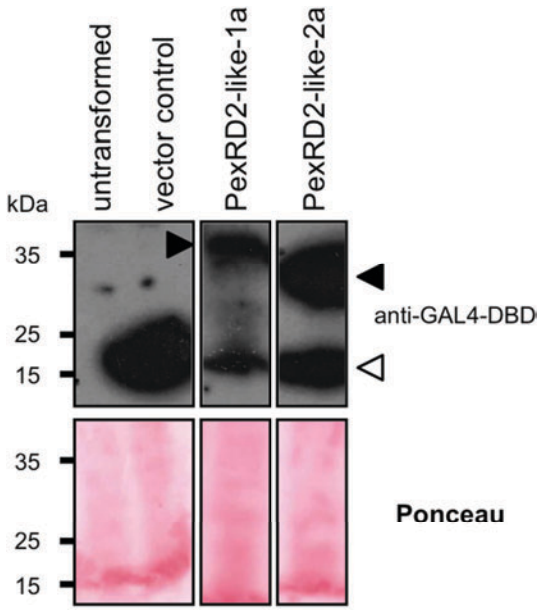

Supplemental Figure 1. PexRD2-like bait proteins are expressed and stable in yeast. Immunoblot analysis using an antibody specific to the DNA-binding domain of GAL4 (anti-GAL4-DBD) and total protein extracts from yeast transformants used in **Figure 2B** confirms expression of both PexRD2-like bait fusion proteins. Arrowheads indicate expected sizes of PexRD2-like-1a bait and PexRD2-like-2a bait (black) or non-specific bands and/or tags (white). Protein loading is confirmed by Ponceau staining.

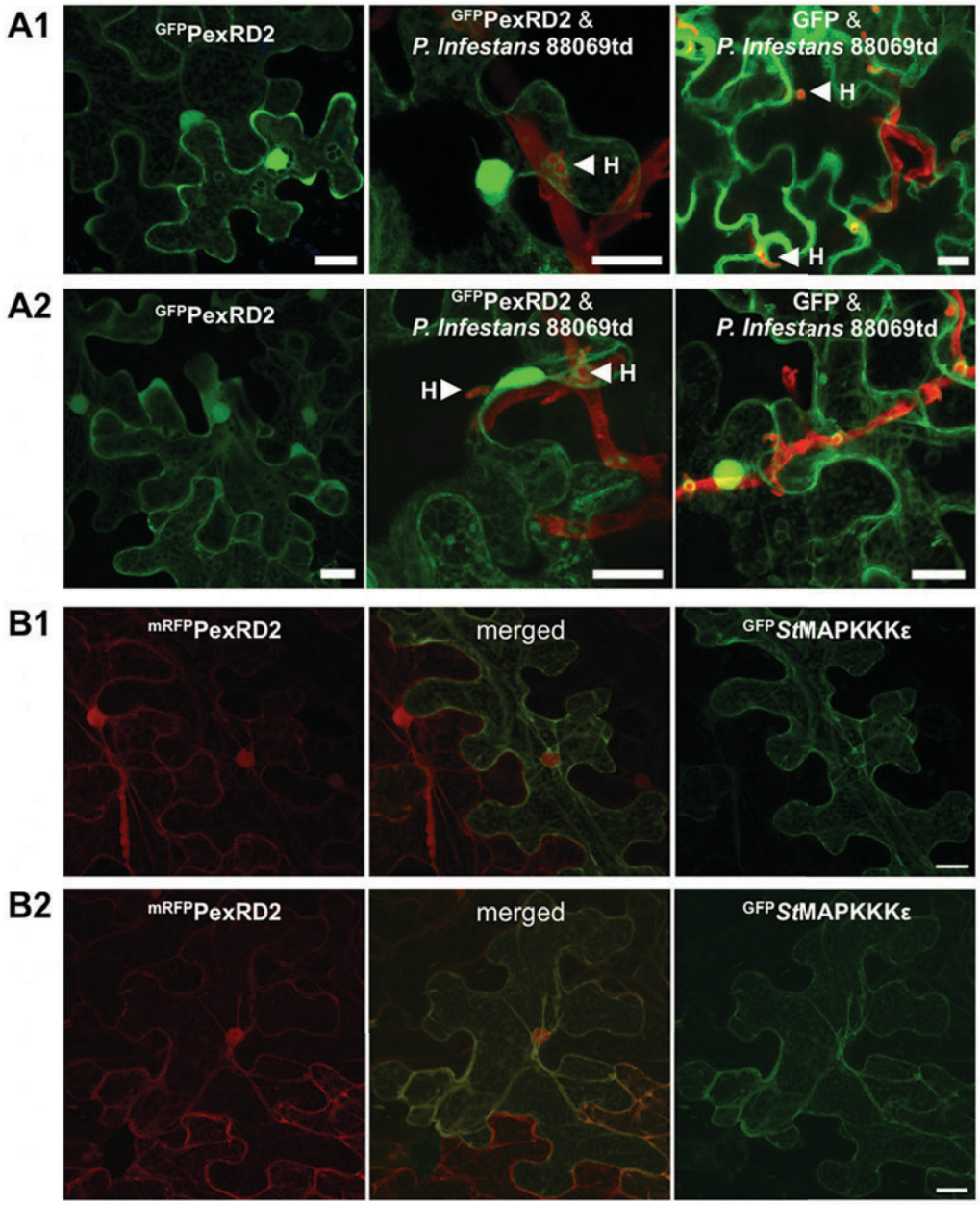

Supplemental Figure 2. PexRD2 and MAPKKKε co-localise in the plant cell cytoplasm. A1 and A2. Confocal images of ^{GFP}PexRD2 in the absence (left) and presence (middle) of *P. infestans* 88069^{td}, and free GFP with *P. infestans* 88069^{td}, shown as a control (right). Haustoria (H) are arrowed. **B1 and B2.** Two independent cells co-expressing ^{mRFP}PexRD2 (left) with ^{GFP}*St*MAPKKKε (right) showing co-localisation in the cytoplasm (merge; middle). Size markers are 20 µm.

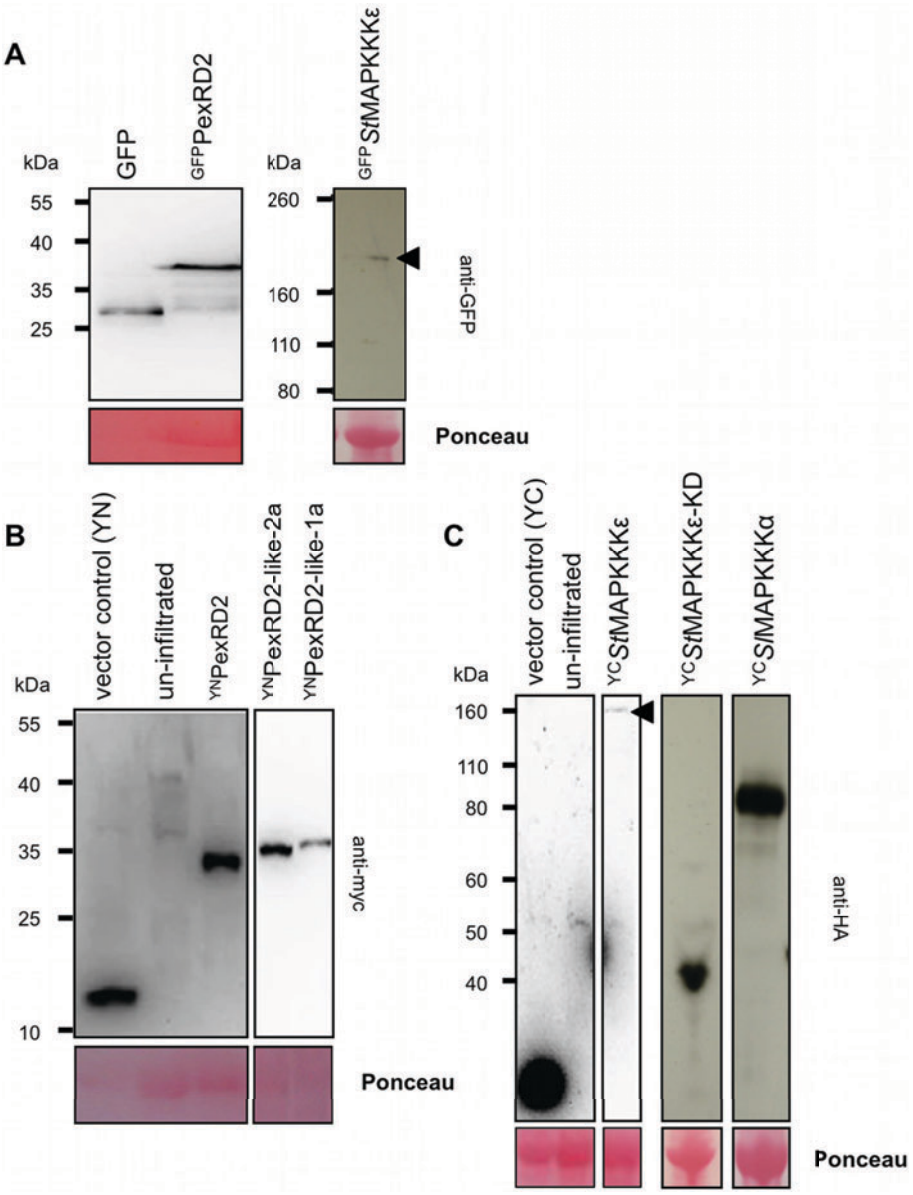

Supplemental Figure 3. Localisation and Split YFP fusion proteins are expressed and stable *in planta*. A. Immunoblot analysis using an anti-GFP antibody on plant protein extracts confirms expression and expected sizes of ^{GFP}PexRD2 and ^{GFP}*St*MAPKKKε (arrowhead indicates ^{GFP}*St*MAPKKKε). **B.** Immunoblots using an anti-myc tag antibody show the expected size bands for ^{YN}PexRD2 and both PexRD2-like family proteins. **C.** Immunoblots using an anti-HA antibody show the expected size bands for ^{YC}*St*MAPKKKε, ^{YC}*St*MAPKKKε-KD and ^{YC}*Sl*MAPKKKα (^{YC}*St*MAPKKKε is indicated by an arrowhead).

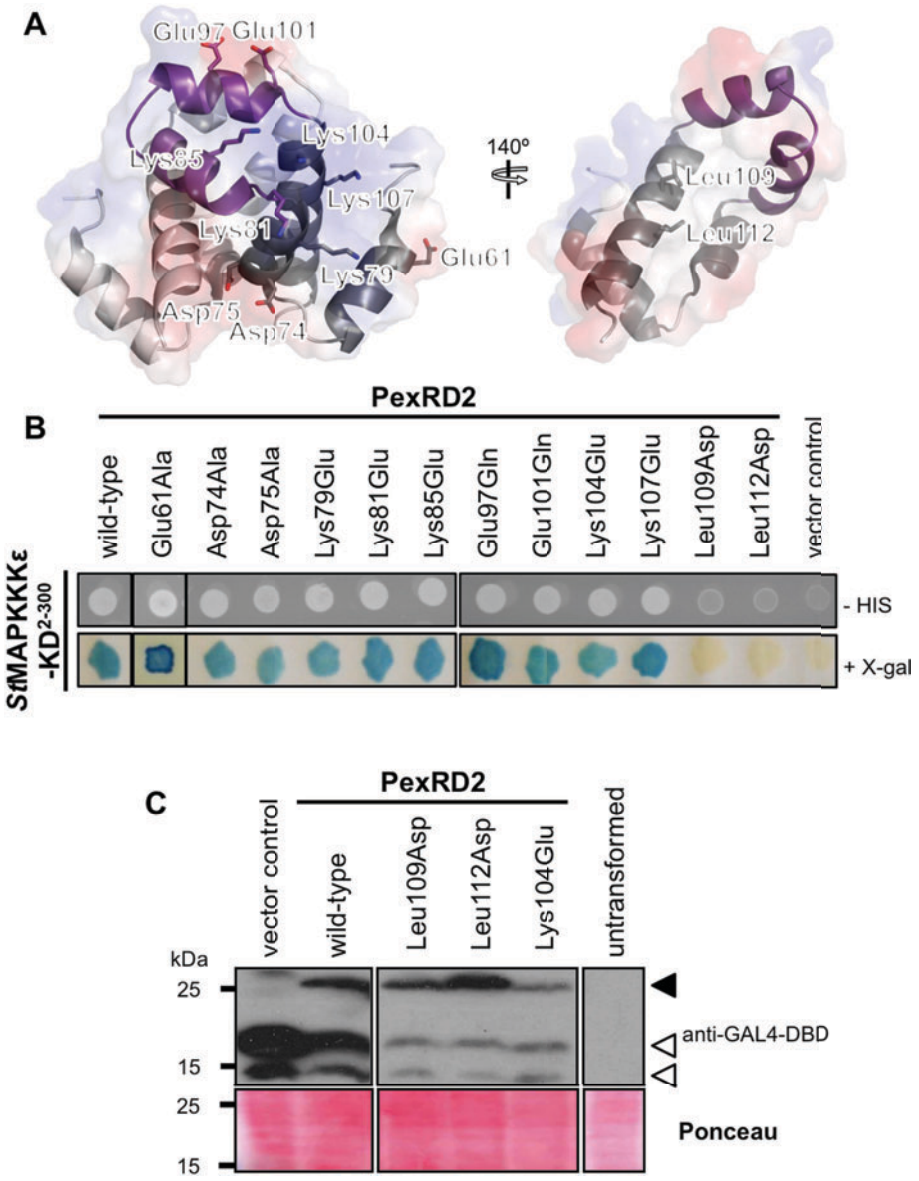

Supplemental Figure 4. Structure-informed point mutants of PexRD2 can disrupt the interaction with MAPKKKε. A. Ribbon diagram of the PexRD2$^{57-121}$ structure (PDB:3ZRG) with transparent electrostatic surface potential displayed. (Left) Structure of PexRD2 dimer, with one monomer coloured in dark grey, to indicate the conserved core of the WY-domain fold, and purple, to highlight the variable region (previously referred to as 'loop-3'). The side-chains of ten surface-presented residues targeted by mutagenesis are shown and labelled appropriately. (Right) A PexRD2 monomer, coloured as described above, but rotated to show the hydrophobic dimerisation interface. The two leucine residues targeted by mutagenesis are shown and labelled. **B.**

Yeast two-hybrid assay showing that only the two mutations in the dimer interface of PexRD2 (Leu109Asp and Leu112Asp) abolish the interaction with the *St*MAPKKKε-KD, as evidenced by the lack of growth on selective media lacking histidine (-HIS) or blue colouration in the presence of X-gal. All point mutations in surface presented residues of PexRD2 did not affect the interaction with *St*MAPKKKε-KD in this assay. **C.** Immunoblot analysis using an antibody specific to the DNA-binding domain of GAL4 (anti-GAL4-DBD) with total protein extracts from yeast transformants used in (B), and an untransformed control, confirms expression of bait fusion proteins. The arrowheads indicate the expected size of PexRD2 bait fusion proteins (black) or non-specific bands and/or tags (white). Protein loading is confirmed by Ponceau staining.

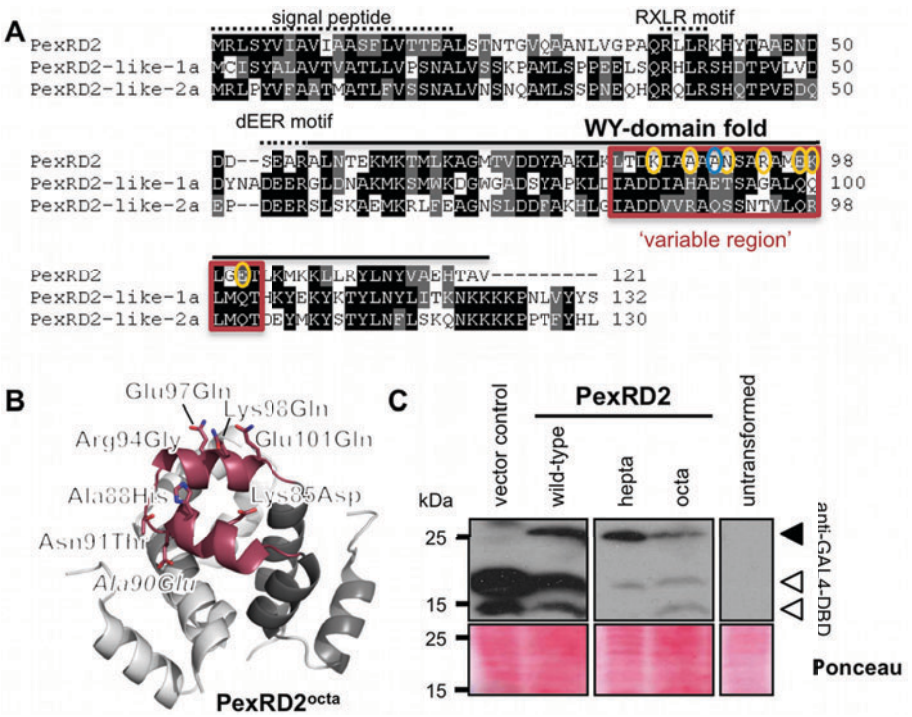

Supplemental Figure 5. Mutations within the structurally variable region of the WY-fold of PexRD2 reduce the interaction with MAPKKKε. A. Sequence alignment of full-length PexRD2, PexRD2-like-1a and PexRD2-like-2a, with features of these proteins labelled. The structurally variable region within the WY-domain-fold of PexRD2 (previously referred to as 'loop-3') is indicated by the maroon box. The seven residues mutated in the PexRD2^{hepta} mutant are circled in yellow, and the additional mutation to generate PexRD2^{octa} is in blue (each mutant replaces the residue in PexRD2 with that found in PexRD2-like-1a). **B.** Ribbon diagram of the PexRD2 structure showing the residues mutated to generate PexRD2^{octa}. The Ala90Glu mutation, unique to PexRD2^{octa}, is labelled in italics. **C.** Immunoblot analysis using an antibody specific to the DNA-binding domain of GAL4 (anti-GAL4-DBD) and total protein extracts from yeast transformants used in **Figure 4** confirms expression of bait fusion proteins. The arrowheads indicate the expected size of PexRD2 bait fusion proteins (black) or non-specific bands and/or tags (white). Protein loading is confirmed by Ponceau staining.

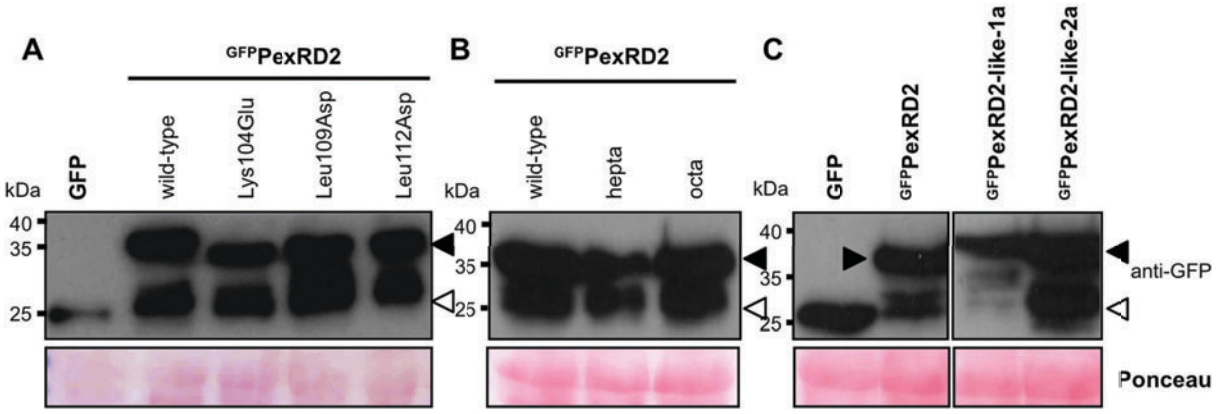

Supplemental Figure 6. GFP-fusion proteins used for *in planta* assays are expressed and stable. Immunoblot analysis using an anti-GFP antibody confirms expression of **A.** point mutants in PexRD2, **B.** PexRD2^{hepta} and PexRD2^{octa}, and **C.** PexRD2-like fusion proteins in *N. benthamiana*. The arrowheads indicate the expected size of PexRD2 fusion proteins (black) or free GFP (white). Protein loading is confirmed by Ponceau staining.

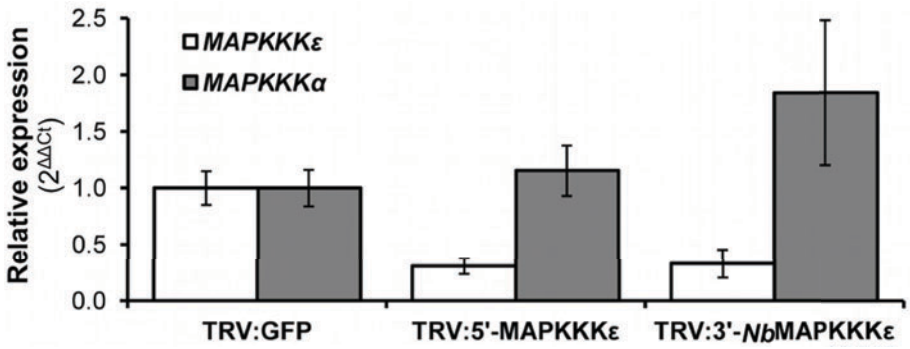

Supplemental Figure 7. Real-Time Quantitative Reverse Transcription PCR (qRT-PCR) confirms specific silencing of *MAPKKKε*. Relative expression of the Nb-*MAPKKKε* and Nb-*MAPKKKα* genes in pooled samples (3 plants per construct) for each TRV:MAPKKKε construct, and with TRV:GFP-treated control samples standardised to 1.0. Analysis was carried out using the ∆/ΔCt method with the endogenous Nb-*EF-1-α* used as an internal control. Data represents two biological repeats (each with three technical repeats) giving similar results.

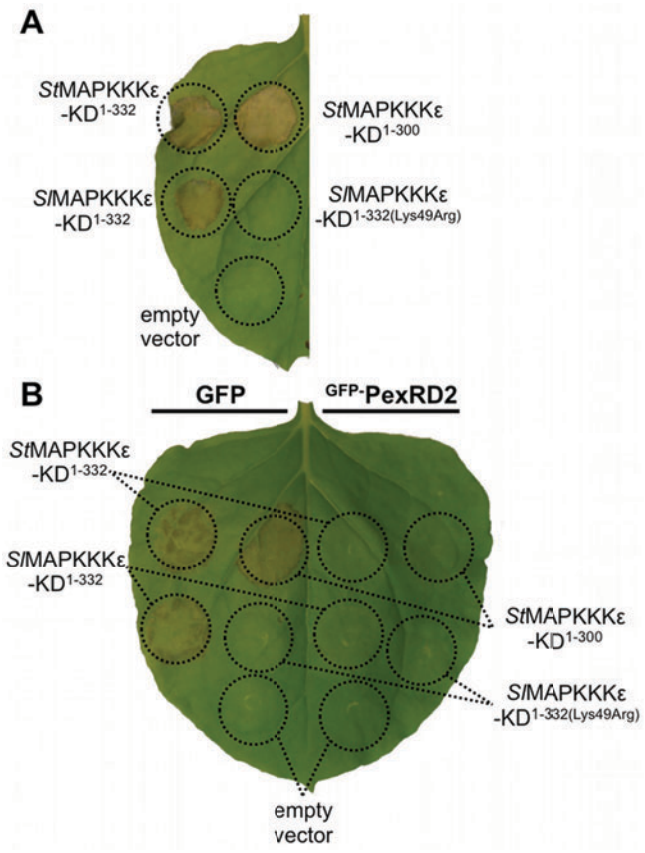

Supplemental Figure 8. The tomato and potato homologues of MAPKKKε trigger cell death that is suppressed by PexRD2. A. Expression of the kinase domain of St-MAPKKKε (*St*MAPKKKε-KD$^{1-332}$ and *St*MAPKKKε-KD$^{1-300}$) in *N. benthamiana* triggers a cell death similar to that of *Sl*MAPKKKε-KD$^{1-332}$. No cell death is triggered by the expression of the kinase inactive mutant (*Sl*MAPKKKε-KD$^{1-332(Lys49Arg)}$) or the pER8 empty vector control. **B.** The cell death triggered by all three active MAPKKKε-KD constructs is suppressed by co-expression with ^{GFP}PexRD2, but not GFP. Images taken at five days post-β-estradiol-treatment to induce expression of the kinases.

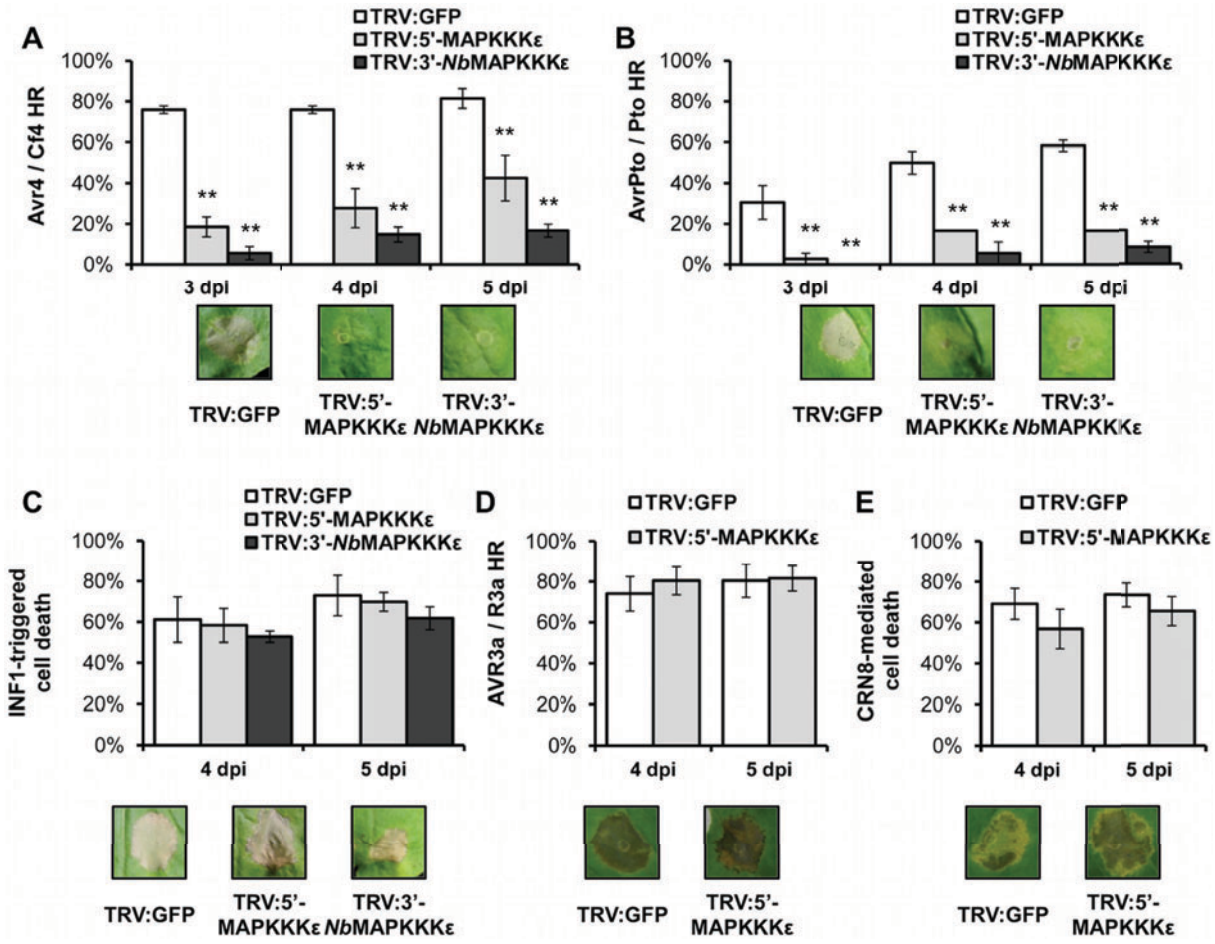

Supplemental Figure 9. VIGS experiments to investigate MAPKKKε-dependent and MAPKKKε-independent cell death events. Virus-induced gene silencing (VIGS) of *MAPKKK*ε in *N. benthamiana* using TRV:5'-MAPKKKε or TRV:3'-*Nb*MAPKKKε reduces the level of hypersensitive response (HR)-associated cell death observed at 3 – 5 days post-agroinfiltration (dpi) following the co-expression of **A.** the *Cladosporium fulvum* effector Avr4 with Cf4 and **B.** the *Pseudomonas syringae* effector AvrPto with Pto. Silencing *MAPKKK*ε does not affect **C.** the cell death triggered by the *P. infestans* PAMP-like elicitin INF1, **D.** the HR following co-expression of the *P. infestans* effector AVR3a^{KI} with R3a, or **E.** the cell death mediated by *P infestans* effector CRN8. Graphs show percentage of infiltration sites with >50% confluent cell death at the time points as indicated. Results are the mean ± SEM from at least three plants. Asterisks indicate values significantly different from the TRV:GFP control at the same time point ($P < 0.01$)

as determined by one-way ANOVA, all other values were not significantly different (ns, $P > 0.05$). Images indicate representative infiltration sites at 6 – 7 dpi.

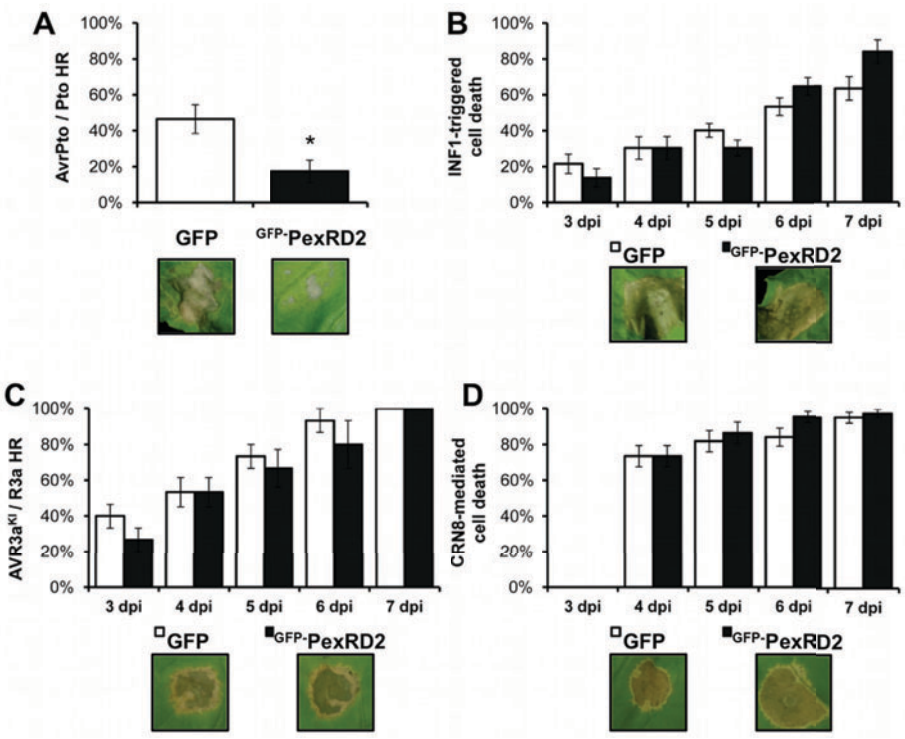

Supplemental Figure 10. PexRD2 suppresses MAPKKKε-dependent AvrPto/Pto hypersensitive response (HR), but not MAPKKKε-independent cell death. A. Co-expression of ^{GFP}PexRD2 with the both the *Pseudomonas syringae* effector AvrPto and tomato resistance protein Pto in *N. benthamiana,* significantly reduces percentage of infiltration sites with >50% confluent cell death at 8 days post-agroinfiltration (dpi), compared to co-expression of the GFP control. **B.** INF1-triggered cell death, **C.** the HR following co-expression of AVR3a^{KI} with R3a and **D.** CRN8-mediated cell death, are all not affected by co-expression with ^{GFP}PexRD2. Results are the mean ± SEM of at least five plants. Asterisk indicates a value significantly different from the GFP control at the same time point ($P < 0.05$) as determined by a t-test, all other values were not significantly different ($P > 0.05$) by one-way ANOVA. Images indicate representative infiltration sites at 7 - 8 dpi.

Supplemental Table 1: Primers used in this study

PexRD2-F	**cacc**atgctctcgacgaacacgggtgttcag
PexRD2-R	tcaaactgctgtgtgttcagccacatagttgagg
PexRD2-57-F	**cacc**atggccctgaatacagagaagatgaaaacg
PexRD2-like-1a-F	**cacc**atgctcgtgagctcaaagc
PexRD2-like-1a-R	ttatgagtagtagacaagattcggcttc
PexRD2-like-2a-F	**cacc**atgctcgtgaactcgaac
PexRD2-like-2a-R	ttataaatggtagaaagtaggtggcttc
MAPKKKε-F	**cacc**tctaggcaaatggcaaatgctg
MAPKKKε-278-R	ttatcaccttgaattttgtatccaaggatg
MAPKKKε-300-R	ttatcaagccgatccatcttcttctatatt
MAPKKKε-373-R	ttatcactcatgaattgctaaagttggaac
MAPKKKε-279-F	**cacc**cgtgctttgcagtcctcactc
MAPKKKε-301-F	**cacc**gtcagagaggcatcaaatga
MAPKKKε-R	ttacaaaactgtgtttatgtggagagc
MAPKKKα-F	**cacc**atgcctgcttggtgg
MAPKKKα-R	ttattaagaatgggtcttgttttg
Xho-MAPKKKε-F	cagctcgagctatgtctaggcaaatggcaaatgc
MAPKKKε-300-*PacI*-R	ggattaattaaagccgatccatcttcttctatatttc
MAPKKKε-332-*PacI*-R	ggattaattaattcaggtggtgccaat
CRN8-F	gagagacccgggacaagtagtgcgcctatttctgatgggacg
CRN8-R	gagagactcgagtcaggcacgtctgtgcttcttgcgcacacc
PexRD2^{hepta}-F	gatattgcacacgcagcaacttctgcaggcgcg
PexRD2^{hepta}-R	cgcgcctgcagaagttgctgcgtgtgcaatatc

Start codons are coloured in green and termination codons in red. **Bold** type indicates CACC sequence required for directional TOPO® cloning. Underlined sequences indicate restriction sites used for cloning.

Supplemental Methods

CONFIRMATION OF PROTEIN EXPRESSION IN YEAST AND PLANT CELLS

Samples of total proteins from yeast transformants containing bait fusion proteins, as used in Y2H assays, were produced using the urea/SDS method described in the Clontech Yeast Protocols Handbook. 20 µL boiled samples were then separated by SDS-PAGE and transferred to PVDF membrane. Immunoblotting was performed using anti-GAL4-DBD HRP-conjugated antibody (Santa Cruz Biotechnology), and detected using a chemiluminescent substrate (Thermo Scientific). See **Supplemental Figures 1, 4 and 5**.

Expression of GFP-fusion proteins in plant cells was confirmed using total protein extracts harvested from leaves 3 dpi. Protein extracts were separated by SDS-PAGE, and transferred to PVDF membranes. Membranes were probed with anti-GFP primary antibodies (Invitrogen), anti-rabbit secondary antibodies conjugated to horseradish peroxidase (Sigma), and a chemiluminescent substrate (Thermo Scientific). See **Supplemental Figures 3 and 6**.

The stability of all fusions was checked by immunoblotting using antibodies to the myc tag (fused to the YN fragment) and the HA tag (fused to the YC fragment). See **Supplemental Figure 3**.

SUB-CELLULAR LOCALISATION OF PEXRD2 AND St-MAPKKKε

Localisation studies

For localisation and co-localisation studies, leaves of 4- to 5-week-old *N. benthamiana* plants were agroinfiltrated singly or in combination at a final OD_{600} of 0.01 (for each strain) with Agrobacteria containing constructs expressing GFP (pB7WGF2) and mRFP

(monomeric RFP, pK7WGR2) fusions to PexRD2 and MAPKKKε. Low infiltration ODs were used for localization studies as these are favoured for fluorescence microscopy, but also reduced the cell death activities of the kinases. Two days after agroinfiltration leaf pieces were imaged using a Zeiss 710 confocal microscope. GFP was excited with a 488 nm laser line and emissions between 500 and 530 nm were collected. mRFP was excited with a 561 nm laser and its emissions were collected between 590 and 620 nm. The stability of the GFP-fusion proteins was checked by immunoblotting (**Supplemental Figure 3**). General cytoplasmic fluorescence was detected in the absence or presence of *P. infestans* infection, using *P. infestans* 88069^{td} expressing a tandem-dimer red fluorescent protein allowing visualization of hyphal growth (**Supplemental Figure 2**). Co-localisation of ^{mRFP}PexRD2 and ^{GFP}*St*MAPKKKε revealed that both proteins reside in the host cytoplasm (**Supplemental Figure 2).**

BIOINFORMATIC ANALYSIS OF POTENTIAL VIGS OFF-TARGETS

VIGS of Nb-*MAPKKKε* has previously been shown to affect specific cell death associated with plant immunity and tests for off-target silencing were negative (Melech-Bonfil and Sessa, 2010). Bioinformatic analyses of the DNA sequences cloned into the pTRV2 vector were performed to identify all 21-nucleotide (21-nt) sequences that displayed the following characteristics, previously identified as predicting high silencing efficiency in mammalian cells and chicken embryos (Ui-Tei et al., 2004). Putative efficient siRNAs had the 5'-end of the antisense strand as an adenine (A) or uracil (U); the first seven bases of the antisense strand including at least five A or U bases; the 5'-end of the sense strand as a guanine (G) or cytosine (C), and a GC-content between 30 – 70%.

These putative siRNAs were then used to find homologous transcripts (targets) in the recently released *Nicotiana benthamiana* draft genome (Bombarely et al., 2012). Since assessments of siRNA specificity suggest that mRNAs with only partial complementarity to a siRNA can also be targeted for destruction (Jackson et al., 2003; Haley and Zamore, 2004), the level of mismatch allowed was varied from zero, perfect

complementarity, up to a maximum of three mismatches. In all cases, no more than a single mismatch was permitted within the so called 'seed region' (positions 2 – 12 from the 5' end) and purine:purine mismatches at position 16 were also excluded, as these had been previously shown to drastically reduce silencing efficiency (Jackson et al., 2006; Schwarz et al., 2006)

The 356-nt insert in TRV:GFP was predicted to contain 32 putative efficient 21-nt siRNAs, whilst the 411-nt insert in TRV:5'-MAPKKKε and the 348-nt insert in TRV:3'-*Nb*MAPKKKε were predicted to contain 43 and 30, respectively. The *N. benthamiana* genome encodes two paralogues of MAPKKKε, Nb-MAPKKKε1 (Melech-Bonfil and Sessa, 2010) and the more recently identified Nb-MAPKKKε2 (Hashimoto et al., 2012), which share 98% DNA and 95% amino acid sequence identity. Unlike TRV:5'-MAPKKKε and TRV:3'-*Nb*MAPKKKε, none of the predicted TRV:GFP-derived siRNAs showed any homology to either MAPKKKε transcript, even when using the highest level of siRNA/site mismatch threshold tested.

As expected, increasing the maximum level of mismatch allowed between the predicted siRNAs and sites in potential target transcripts increased the number of predicted putative off-targets. At the maximum level of mismatch tested, TRV:5'-MAPKKKε, TRV:3'-*Nb*MAPKKKε and TRV:GFP had predicted totals of 45, 16 and 20 putative off-targets, respectively. Analysis of these 81 putative off-target sequences revealed that they are all unique to their respective silencing constructs. Only the two paralogues of Nb-*MAPKKKε* are targeted by both TRV:5'-MAPKKKε and TRV:3'-*Nb*MAPKKKε, but importantly not TRV:GFP.

RNA isolation and qRT-PCR

Total RNA was extracted from VIGS plant samples using a Plant RNeasy Kit (Qiagen). First strand cDNA was generated from 1 µg RNA using Superscript II RNaseH Reverse Transcriptase (Invitrogen) and an oligo dT primer according to the manufacturers' instructions. Quantitative RT-PCR was performed using Power SYBR Green (Applied Biosystems) and a Chromo4 thermal cycler (MJ Research) with the following primers

(MAPKKKε: tgaagatgatctctggtctgtca/ttccactttcctgctttcgt) (MAPKKKα: ttcgttggtgctctctttca/cagggtggctttgaacttg) (endogenous control EF-1α: tggacacagggacttcatca/caagggtgaaagcaagcaat). Data was analysed using Opticon Monitor 3 software and calculations and statistical analysis were performed as described previously (Lacomme et al., 2003). See **Supplemental Figure 7**.

SUPPLEMENTAL REFERENCES

Bombarely, A., Rosli, H.G., Vrebalov, J., Moffett, P., Mueller, L.A., and Martin, G.B. (2012). A draft genome sequence of Nicotiana benthamiana to enhance molecular plant-microbe biology research. Mol Plant Microbe Interact **25,** 1523-1530.

Haley, B., and Zamore, P.D. (2004). Kinetic analysis of the RNAi enzyme complex. Nature structural & molecular biology **11,** 599-606.

Hashimoto, M., Komatsu, K., Maejima, K., Okano, Y., Shiraishi, T., Ishikawa, K., Takinami, Y., Yamaji, Y., and Namba, S. (2012). Identification of three MAPKKKs forming a linear signaling pathway leading to programmed cell death in Nicotiana benthamiana. BMC Plant Biol **12,** 103.

Jackson, A.L., Burchard, J., Schelter, J., Chau, B.N., Cleary, M., Lim, L., and Linsley, P.S. (2006). Widespread siRNA "off-target" transcript silencing mediated by seed region sequence complementarity. RNA **12,** 1179-1187.

Jackson, A.L., Bartz, S.R., Schelter, J., Kobayashi, S.V., Burchard, J., Mao, M., Li, B., Cavet, G., and Linsley, P.S. (2003). Expression profiling reveals off-target gene regulation by RNAi. Nature biotechnology **21,** 635-637.

Melech-Bonfil, S., and Sessa, G. (2010). Tomato MAPKKKepsilon is a positive regulator of cell-death signaling networks associated with plant immunity. Plant J **64,** 379-391.

Schwarz, D.S., Ding, H., Kennington, L., Moore, J.T., Schelter, J., Burchard, J., Linsley, P.S., Aronin, N., Xu, Z., and Zamore, P.D. (2006). Designing siRNA That Distinguish between Genes That Differ by a Single Nucleotide. PLoS Genet **2,** e140.

Ui-Tei, K., Naito, Y., Takahashi, F., Haraguchi, T., Ohki-Hamazaki, H., Juni, A., Ueda, R., and Saigo, K. (2004). Guidelines for the selection of highly effective siRNA sequences for mammalian and chick RNA interference. Nucleic acids research **32,** 936-948.